Force-Gradient Sensing and Entanglement via Feedback Cooling of Interacting Nanoparticles

Henning Rudolph,[1] Uroš Delić,[2] Markus Aspelmeyer,[2,3] Klaus Hornberger,[1] and Benjamin A. Stickler[1]
[1]University of Duisburg-Essen, Faculty of Physics, Lotharstraße 1, 47057 Duisburg, Germany
[2]University of Vienna, Faculty of Physics, Boltzmanngasse 5, A-1090 Vienna, Austria
[3]Austrian Academy of Sciences, Institute for Quantum Optics and Quantum Information (IQOQI) Vienna, Boltzmanngasse 3, A-1090 Vienna, Austria

(Received 28 April 2022; accepted 7 October 2022; published 2 November 2022)

We show theoretically that feedback cooling of two levitated, interacting nanoparticles enables differential sensing of forces and the observation of stationary entanglement. The feedback drives the two particles into a stationary, nonthermal state which is susceptible to inhomogeneous force fields and which exhibits entanglement for sufficiently strong interparticle couplings. We predict that force-gradient sensing at the zepto-Newton per micron range is feasible and that entanglement due to the Coulomb interaction between charged particles can be realistically observed in state-of-the-art setups.

DOI: 10.1103/PhysRevLett.129.193602

Introduction.—The key to precision sensing lies in a thorough isolation from environmental perturbations. Levitating nanoparticles with lasers in ultrahigh vacuum presents a promising platform, as optical fields grant precise control over the particle motion, while the environment can be efficiently shielded [1,2]. Their exquisite isolation renders these systems promising for future force and torque sensing technologies [3–5], for tests of the quantum superposition principle with increasingly macroscopic objects [6–8], for the observation of mechanical entanglement [9–16], for explorations of physics beyond the standard model [17–19] and for probing the quantumness of gravity [20–25].

Levitated particles have been cooled to the motional ground state by two different methods [26–30]. Coherent scattering cooling uses the scattering of red-detuned tweezer light into a high finesse cavity [31–34], efficiently reducing the effect of laser phase noise heating [35] and holding the prospects of also cooling rotational degrees of freedom [36]. In contrast, feedback cooling [37–42] uses the information extracted from the Rayleigh-scattered tweezer light to apply feedback forces and cool the particle motion. Feedback cooling circumvents limitations posed by shot noise if the information leaking out of the system can be detected and utilized sufficiently well [27,28]. Feedback control of levitated particles has also been proposed for optimal control of their quantum state [14,15,27,39,43], which is ultimately limited by the computational resources of the feedback loop.

In this Letter, we show theoretically how feedback techniques can drive two interacting nanoparticles into a stationary state close to the two-particle ground state. Our calculations demonstrate that this enables sensing of local force gradients on the zepto-Newton per micrometer scale and that the interaction leads to squeezing of the relative motion. We predict under which conditions the two particles generate stationary Gaussian entanglement, for instance due to Coulomb interaction, where feedback cooling replaces the cryogenic cooling on which clamped

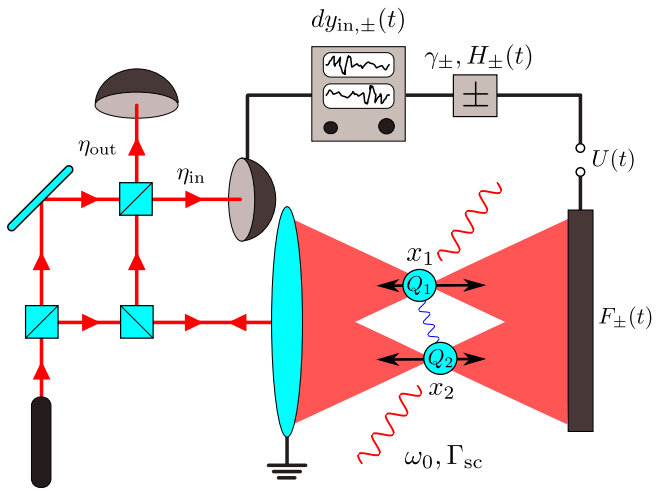

FIG. 1. Two spherical, charged nanoparticles (blue spheres) are levitated in two tweezer traps with identical trapping frequencies ω_0 and recoil heating rates Γ_{sc}, whose collimation lens is grounded. The particles motion along the optical axis $x_{1,2}$ is detected with an efficiency η_{in} and the measurement signals of the sum and difference modes $dy_{\mathrm{in},\pm}(t)$ are monitored. The signals are convoluted with the feedback functions $H_\pm(t)$ and multiplied with damping constants $\gamma_\pm$ to apply voltage $U(t)$, leading to feedback forces $F_\pm$. A second detector measures the particles motion with efficiency η_{out}, which is not part of the feedback loop, and is additionally used to detect external forces and interparticle entanglement.

experiments typically rely [44–46]. Interparticle coupling due to the Coulomb force has been recently studied experimentally with levitated nanoparticles [47,48]. Our scheme is feasible with state-of-the-art technology [27,28], requiring merely that both normal modes of the two-particle motion can be measured and feedback cooled individually, as recently accomplished for noninteracting particles [49].

Feedback master equation.—The proposed experimental setup is depicted in Fig. 1. Two nanoparticles of mass m, electric susceptibility $\chi_e = 3(\varepsilon_r - 1)/(\varepsilon_r + 2)$, dielectric permittivity ε_r, mass density ϱ, and volume V are trapped in two parallel tweezers with approximately equal wave numbers k, Rayleigh ranges x_R, and drive powers P. Our assumption of (almost) equal particles and tweezers, which is for simplicity and ease of notation, can be readily lifted. The tweezer foci are separated by a distance d and lie in the plane perpendicular to both tweezer propagation directions. The light scattered off each particle is collected and distributed among four homodyne detectors: two in-loop detectors with efficiencies η_{in} responsible for feedback cooling the particles, and two out-of-loop detectors with efficiencies η_{out} required for independently monitoring the particle motion and for force measurements. For simplicity, we assume the tweezers to be detuned from each other to avoid interference between the tweezer outputs in the detection. Otherwise, an appropriate spectral filter would be required to access all normal modes of the mechanical system.

The particle motion perpendicular to the optical axis is assumed to be sufficiently cooled that coupling to the motion along the optical axis can be neglected [27,28]. In that case we may restrict the discussion to the coordinates along the optical axis, denoted by $x_{1,2}$.

For harmonically trapped particles, whose diameter is much smaller than the optical wavelength, the trapping frequency is given by $\omega_0 = \sqrt{\chi_e k P/\pi c \varrho x_R^3}$. Incoherent scattering of tweezer photons leads to recoil heating with the rate [34,50]

$$\Gamma_{\mathrm{sc}} = \omega_0 \frac{\chi_e k^5 V x_R^2}{60\pi}\left[2 + 5\left(1 - \frac{1}{k x_R}\right)^2\right]. \tag{1}$$

The particles hold excess charges $Q_{1,2}$, $|Q_1| \neq |Q_2|$, enabling one to apply the feedback forces $F_{1,2}(t)$ via a homogeneous electric field and thereby to cool the motion of both particles. The two particles interact via the Coulomb force, which for small displacements from the tweezer foci is given by $V_{\mathrm{int}} = m\omega_0 g(x_1 - x_2)^2$. The coupling constant can be expressed as $g = -Q_1 Q_2/8\pi m\omega_0 \varepsilon_0 d^3$, so that $g > 0$ for attractive interactions and $g < 0$ for repulsion. In addition to this electrostatic interaction, the particles might interact via conservative optical binding forces [48], which would increase the coupling constant g. Note that the electrostatic interaction also displaces the particles along their connecting axis, potentially changing the effective trapping frequency and recoil rate [50].

Our aim is to measure the difference between the two forces $K_{1,2}(t)$, which are acting on the two particles due to an additional inhomogeneous field. The Hamiltonian describing the particle dynamics can be expressed in terms of the sum and difference motion operators, $x_\pm = (x_2 \pm x_1)/\sqrt{2}$ and $p_\pm = (p_2 \pm p_1)/\sqrt{2}$ as

$$H = \sum_{s=\pm}\left(\frac{p_s^2}{2m} + \frac{m\omega_s^2}{2}x_s^2 - F_s(t)x_s - K_s(t)x_s\right). \tag{2}$$

Here, we defined the sum and difference mode frequencies $\omega_+ = \omega_0$ and $\omega_-^2 = \omega_0^2 + 4g\omega_0$ as well as the mean and offset forces $F_\pm(t) = [F_2(t) \pm F_1(t)]/\sqrt{2}$ and $K_\pm(t) = [K_2(t) \pm K_1(t)]/\sqrt{2}$. The center-of-mass motion of the two particles thus serves to measure the mean external force while their differential motion senses the mean force gradient.

The homodyne detectors monitor the particle motion by generating the measurement outcomes $dy_{1,2}^r$, where $r \in \{\mathrm{in}, \mathrm{out}\}$ denotes the in-loop and out-of-loop measurement channels. Given the two-particle state ρ and combining the measurement outcomes to $dy_{r\pm} = (dy_2^r \pm dy_1^r)/\sqrt{2}$ yields [57]

$$dy_{rs} = \langle x_s\rangle dt + \frac{L}{\sqrt{\eta_r}}dW_{rs}, \tag{3}$$

where $s \in \{+,-\}$. Here, $\langle\cdot\rangle = \mathrm{tr}(\rho\cdot)$ denotes the quantum expectation value and dW_{rs} are statistically independent Wiener processes, $\mathbb{E}[dW_{rs}] = 0$ and $\mathbb{E}[dW_{rs}dW_{r's'}] = \delta_{rr'}\delta_{ss'}dt$, where $\mathbb{E}[\cdot]$ is the ensemble average over the measurement outcomes. The Wiener increments model the photon shot noise due to the local oscillators used for the homodyne detection. The parameter $L^2 = \hbar/8m\omega_0\Gamma_{\mathrm{sc}}$ describes the accuracy of the position measurements as determined by the recoil heating rate, and the quantum efficiencies η_r quantify how much information can be extracted from the scattering fields, taking into account that the information is not uniformly distributed for all scattering directions [27,28]. Note that the setup implies $\eta_{\mathrm{in}} + \eta_{\mathrm{out}} \leq 1$, see Fig. 1.

The quantum master equation for the two-particle state ρ conditioned on the homodyne detection of the scattered light (called the *conditional* state) reads [50,57]

$$d\rho = -\frac{i}{\hbar}[H,\rho]dt - \sum_{s=\pm}\left(\frac{D_g}{\hbar^2} + \frac{1}{8L^2}\right)[x_s,[x_s,\rho]]dt + \sum_{r=\mathrm{in,out}}\frac{\sqrt{\eta_r}}{2L}\sum_{s=\pm}\{x_s - \langle x_s\rangle,\rho\}dW_{rs}. \tag{4}$$

Here, we included the impact of residual gas collisions with diffusion constant $D_g = \gamma_g m k_B T_g$, where γ_g denotes the gas damping constant and T_g the gas temperature.

The deterministic part of Eq. (4) describes the coherent time evolution of the system induced by the Hamiltonian (2) as well as the momentum diffusion due to gas collisions and photon recoil. The stochastic term, which is nonlinear in the particle state, accounts for the fact that measuring the scattered fields drives the two-particle quantum state into a product of Gaussian states in the sum and difference modes, conditioned on the measurement results (3). Averaging Eq. (4) over all possible measurement outcomes (and setting $F_\pm = 0$) yields the master equation for a particle diffusing due to recoil heating and gas collisions [34,58]. Note that the stochastic term effectively reduces the recoil heating and decoherence since a fraction η_r of scattered photons is not irretrievably lost [50].

Force-gradient sensing at the standard quantum limit.— We now follow the cold-damping scheme [28,59] and filter the measurement outcomes $dy_{\mathrm{in},s}$ with a feedback filter function $H_s(t)$, that serves as an approximate differentiator [28,59,60] to mimic linear-velocity damping. Denoting the tunable feedback damping rates by γ_s, the feedback forces can be written as an Itô stochastic integral

$$F_s(t) = -m\gamma_s \int_{-\infty}^{\infty} dy_{\mathrm{in},s}(t') H_s(t - t'). \tag{5}$$

Thus, both the position information and the measurement noise are filtered and fed back onto the particle motion. Especially for large feedback rates, this may impact the achievable steady-state energy and the noise floor of force-gradient measurements [59].

We are now in the position to compute the detected in-loop and out-of-loop power spectral densities (PSD) of the mechanical normal modes. In the Supplemental Material [50] we show that

$$S_{rs}[\omega] = \frac{|\chi_s[\omega]|^2}{2\pi m^2}(2\pi S_{K_s K_s}[\omega] + \mathcal{N}_{rs}[\omega]), \tag{6}$$

with the mechanical susceptibilities $\chi_s[\omega] = (\omega_s^2 - \omega^2 + \gamma_s\sqrt{2\pi}H_s[\omega])^{-1}$ and the noise spectra

$$\mathcal{N}_{rs}[\omega] = 2D_g + \frac{\hbar^2}{4L^2} + m^2L^2\left[\frac{|\chi_s[\omega]|^{-2}}{\eta_r} \mp 2\pi\frac{\gamma_s^2}{\eta_{\mathrm{in}}}|H_s[\omega]|^2\right], \tag{7}$$

where the negative (positive) sign applies to the in-loop (out-of-loop) PSD.

The minimal force K_s detectable with the PSDs (6) is determined by the noise spectra (7). Here, the first two terms describe noise due to gas collisions and measurement backaction (shot noise), while the second line describes imprecision noise of the measurement and noise from feeding the in-loop measurement noise back onto the particle motion.

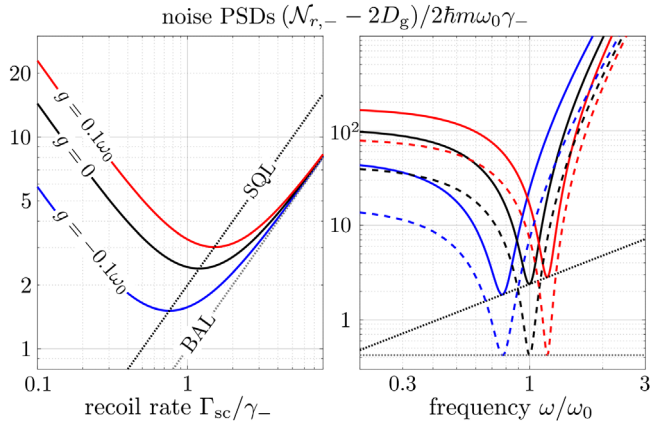

FIG. 2. Normalized noise PSDs (7) of the difference mode for different coupling constants g. Left: $\mathcal{N}_{\mathrm{out},-}$ as a function of the recoil heating rate Γ_{sc} on resonance ($\omega = \omega_-$). Right, solid: $\mathcal{N}_{\mathrm{out},-}$ as function of the frequency ω for the fixed recoil rate $\Gamma_{sc}/\gamma_- = \omega_-\sqrt{1/\eta_{\mathrm{in}} + 1/\eta_{\mathrm{out}}}/4\omega_0$, chosen to minimize the noise on resonance. Right, dashed: the same for $\mathcal{N}_{\mathrm{in},-}$ but with the choice $\Gamma_{sc}/\gamma_- = 1/4\sqrt{\eta_{\mathrm{in}}}$. The damping rate is always $\gamma_- = \omega_0/10$ and the in- and out-of-loop efficiencies are $\eta_{\mathrm{in}} = 0.35$ and $\eta_{\mathrm{out}} = 0.05$, respectively. The black solid curve ($g = 0$) is also the noise PSD of the sum mode. The black dotted lines connect the minima of all possible $\mathcal{N}_{\mathrm{out},-}$ curves and therefore mark the standard quantum limit (SQL) at resonance. The gray dotted lines describe backaction-limited (BAL) detection at resonance, connecting all dashed lines on the right.

At resonance, the in-loop signal is only backaction limited ($D_g = 0$ in the following) due to squashing of the feedback noise [59], irrespective of γ_s. In contrast, the minimal force detectable with the out-of-loop signal at resonance is obtained by choosing γ_s as small as technically feasible and minimising with respect to the measurement accuracy. This yields $L^2 \propto 1/\gamma_s$ and

$$\mathcal{N}_{\mathrm{out},s}[\omega_s]|_{\mathrm{SQL}} = \hbar m\omega_0\gamma_s e^{-2\kappa_s}\sqrt{\frac{1}{\eta_{\mathrm{in}}} + \frac{1}{\eta_{\mathrm{out}}}}, \tag{8}$$

with the (squeezing) parameter $\kappa_s = \log(\omega_s/\omega_0)/2$. As $\eta_{\mathrm{in}} + \eta_{\mathrm{out}} \leq 1$, the minimum detectable force is bounded from below by $2\hbar m\omega_s\gamma_s$, which is reached for $\eta_{\mathrm{in}} = \eta_{\mathrm{out}} = 1/2$. Figure 2 shows that the SQL of gradient force sensing can drop below the corresponding SQL of two noninteracting particles [61], as given by $g = 0$. Measurements below the SQL of uncoupled oscillators can be achieved if the interaction is repulsive, and therefore for $\omega_- < \omega_0$, implying higher force susceptibilities. If the SQL cannot be achieved at a given γ_s, the measurement is still backaction limited.

The force sensitivity of the out-of-loop spectra can be estimated for the experimental setting in Ref. [27] by choosing γ_s and L such that the SQL is reached, as $10^{-20}\mathrm{N}/\sqrt{\mathrm{Hz}}$, which is about one order of magnitude above the backaction limit. This implies a force gradient sensitivity on the zepto-Newton per micrometer scale for particles levitated at micrometer separations [48].

Gaussian entanglement of nanoparticles.—For sufficiently strong coupling, the setup in Fig. 1 can also be used to prepare and observe stationary Gaussian entanglement between the two particles in the absence of external forces $K_s = 0$. Specifically, the feedback loop drives the two particles into a nonthermal stationary state, which exhibits Gaussian entanglement due to the Coulomb interaction, as quantified by the logarithmic negativity [62] of the unconditional two-particle state $\mathbb{E}[\rho]$. The continuous observation of the particle motion effectively reduces the recoil heating rate significantly below the Coulomb coupling rate [50], so that entanglement can be generated and observed by continuously driving the two-particle state into a product of Gaussians in the sum and difference modes.

Introducing dimensionless position and momentum quadratures via $x_s = \sqrt{\hbar/m\omega_0}X_s$ and $p_s = \sqrt{\hbar m\omega_0}P_s$, one can write the elements of the unconditional covariance matrix as a function of the net heating rate $\Gamma = \Gamma_{\mathrm{sc}} + \gamma_g k_B T_g/\hbar\omega_0$ and of the effective detection efficiency $\eta_{\mathrm{eff}} = \eta_{\mathrm{in}}\Gamma_{\mathrm{sc}}/\Gamma$, which describes the detectable fraction of the net information leaving the system. Here, we set $\eta_{\mathrm{out}} = 0$ for simplicity, which is sufficient for estimating the achievable entanglement as typically $\eta_{\mathrm{in}} \gg \eta_{\mathrm{out}}$. To maximize the logarithmic negativity, we consider weak measurements, $\Gamma \ll \omega_s$. In this case one can approximate the nonvanishing elements of the dimensionless covariance matrix as [50]

$$\mathbb{E}[\langle X_s^2\rangle] = \frac{\gamma_s}{16\eta_{\mathrm{eff}}\Gamma} + \frac{\omega_0^2\Gamma}{\omega_s^2\gamma_s} \tag{9a}$$

$$\mathbb{E}[\langle P_s^2\rangle] \approx \frac{\omega_s^2}{16\eta_{\mathrm{eff}}\omega_0^2\Gamma}\gamma_s + \frac{\Gamma}{\gamma_s} + \frac{\Omega_s\gamma_s^2}{16\eta_{\mathrm{eff}}\omega_0^2\Gamma} \tag{9b}$$

$$\mathbb{E}\left[\frac{1}{2}\langle X_s P_s + \mathrm{H.c.}\rangle\right] \approx \frac{\gamma_s}{4\sqrt{\eta_{\mathrm{eff}}}\omega_s}, \tag{9c}$$

where we neglect higher orders in Γ/ω_s and introduce the filter bandwidths [50]

$$\Omega_s = \frac{1}{\pi}\int_{-\infty}^{\infty} d\omega f_s^2[\omega]. \tag{10}$$

They must exceed the spectral width of the mechanical motion $\Omega_s \gg \gamma_s$ to ensure efficient cooling. Physically, the filter bandwidths appear in (9) due to the high frequency fluctuations of the particle momenta originating from feeding back the time derivative of the measurement noise onto the particle dynamics. The optimal choice of the feedback rates for entangling the motion will lead to $\gamma_s \propto \Gamma$, so that $\Omega_s \gg \Gamma$ [50]. Note that neither the conditional nor the unconditional two-particle state are thermal.

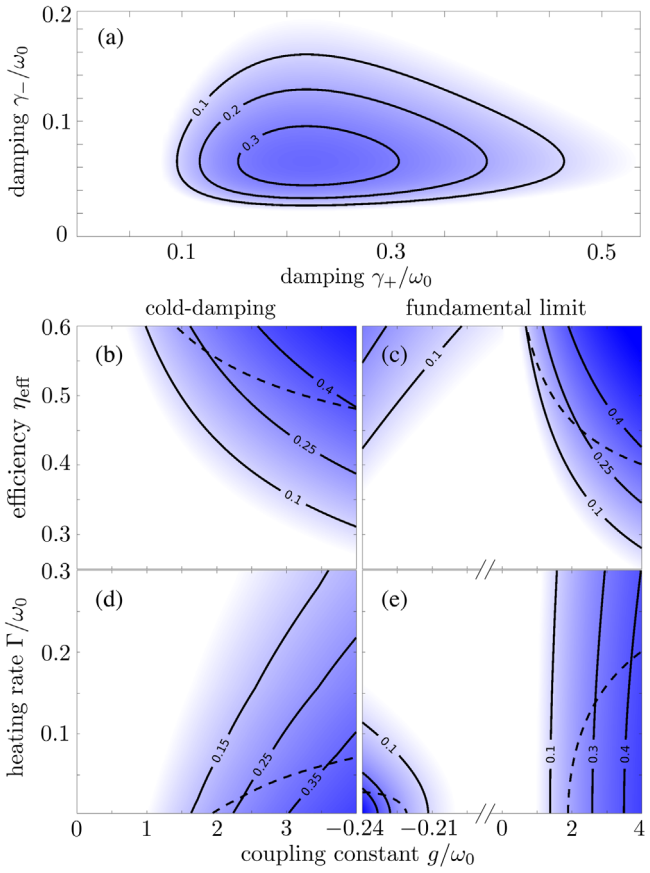

FIG. 3. (a) Logarithmic negativity of two interacting, feedback-cooled nanoparticles as a function of the damping constants γ_s for an effective detection efficiency of $\eta_{\mathrm{eff}} = 0.45$, a net heating rate of $\Gamma = 0.1\omega_0$, and a coupling constant of $g = 4\omega_0$. (b),(d) Logarithmic negativity of the unconditional state as a function of the coupling constant and of the effective detection efficiency or the net heating rate, respectively. The plots are calculated for $\Omega_s = \omega_0$ and at the optimal choice of the damping rates γ_s. (c),(e) Logarithmic negativity of the conditional state. The dashed black lines indicate the violation of the Duan criterion, which is a weaker entanglement criterion than the logarithmic negativity. (b),(c) are calculated for $\Gamma = \omega_0/10$, while (d),(e) assume $\eta_{\mathrm{eff}} = 0.45$. The unconditional negativity (b),(d) can be realized by cold-damping feedback [28], while the conditional negativity (c),(e) can be reached by Kalman filtering [27].

In the limit of weak measurements, $\Gamma \ll \omega_s$, the particles get entangled whenever the detection efficiency exceeds the ratio of the normal mode frequencies, $\eta_{\mathrm{eff}} > \omega_</\omega_>$ [50]. At finite measurement strengths, the finite filter bandwidth always impairs the creation of entanglement. Using the exact unconditional covariance matrix [50], the logarithmic negativity is depicted in Fig. 3(a) as function of the two

damping constants γ_s and in Figs. 3(b) and 3(d) as a function of the heating rate, the detection efficiency, and the coupling constant, numerically maximized over γ_s. The plot shows that entanglement can be observed if either the detection efficiency or the coupling constant is sufficiently large. Negative coupling constants can never lead to entanglement for realistic parameters in the cold-damping cooling scheme, since they increase bandwidth-induced fluctuations in Eq. (9), see Ref. [50]. The logarithmic negativity of the conditional stationary state is shown in Figs. 3(c) and 3(e), demonstrating that Kalman filtering can in principle create entanglement even at negative coupling rates [27].

Discussion.—The presented force sensing and entanglement schemes require the ability to feedback cool both normal modes individually. For short interparticle distances, the easiest way to achieve this is by applying a homogeneous electric field [27,28,40,59,60], implying that the particle charges must be distinct, $|Q_1| \neq |Q_2|$, to ensure that the feedback acts on both normal modes. Alternatively, all optical cold damping schemes have been demonstrated recently [30,49]. To avoid feedback-induced coupling between the normal modes, the bandwidths Ω_s of the filter functions must be sufficiently narrow [63], $\Omega_s < |\omega_+ - \omega_-|$, and the damping rates sufficiently small, $\gamma_s < |\omega_+ - \omega_-|$.

To show that the presented scheme is feasible, we evaluate it for realistic experimental parameters. A silica sphere ($\chi_e = 0.8$, $\varrho = 1850\ \mathrm{kg/m^3}$) with a diameter of 90 nm, trapped in a laser beam with a wavelength of $2\pi/k = 1064$ nm, a power of $P = 300$ mW and a Rayleigh range of $x_R = 1.21$ μm, experiences a trapping frequency of $\omega_0/2\pi = 108$ kHz and a recoil heating rate of $\Gamma_{\mathrm{sc}} = \omega_0/10$. In a nitrogen atmosphere with a temperature of $T_g = 300$ K and a pressure of 10^{-8} mbar the gas damping constant is $\gamma_g/2\pi = 10$ μHz [64] and the net heating rate $\Gamma/2\pi = 11.4$ kHz. If the in-loop efficiency is $\eta_{\mathrm{in}} = 0.4$, which is slightly more ambitious than in [27], the effective detection efficiency is $\eta_{\mathrm{eff}} = 0.38$ (backaction-dominated regime). It follows from Fig. 3(b) that the coupling constant should be at least about $g > 2.5\omega_0$ to achieve entanglement, which can be reached if the particle separation is about $d = 2$ μm and both particles are charged with about 250 elementary charges, which is in reach of present-day experiments [48]. Note that stable trapping of oppositely charged particles may require compensating their steady-state displacement due to the Coulomb interaction. This can be easily done, e.g., by applying a homogeneous electrostatic field along the axis connecting the tweezer foci, which might modify the trapping frequency and recoil rate [50].

To illustrate the force sensitivity and spatial resolution, we note that these parameters would allow for the detection of the force difference due to a single electron placed in the plane of the two tweezers, at an angle of 45° and a distance of 10 μm from the particles, oscillating with frequency ω_- and amplitude 1 μm at a Q factor of 10. The spatial resolution is determined by the interparticle distance, which can in principle be controlled with an accuracy of 8 nm [31].

The discussed schemes can be adapted to Kalman filtering of the mechanical motion [27], which may lead to lower motional temperatures and therefore to better sensing precision and stronger entanglement. It also holds the prospect of eliminating the requirement $|\omega_+ - \omega_-| > \Omega_s$, as no additional noise is directly fed into the particle motion.

In conclusion, we presented a scheme to measure and feedback cool two levitated particles interacting via Coulomb forces, and showed how this can give rise to differential force sensing and entanglement of levitated particles. Recent experimental progress [27,28,47–49] suggests that it can be realized with state-of-the-art technology. As a major benefit, the presented feedback-based entanglement scheme significantly reduces the requirements on environmental isolation in comparison to pulsed approaches [9,14,15]. Moreover, our Letter paves the way for resolving force fields at the zepto-Newton per micrometer scale, with possible applications for explorations of physics beyond the standard model [17–19] and may well find applications in other setups requiring quantum feedback of multiple mechanical modes.

We thank Lorenzo Magrini for helpful discussions. H. R., K. H., and B. A. S. acknowledge funding by the Deutsche Forschungsgemeinschaft (DFG, German Research Foundation)–439339706. U. D. and M. A. acknowledge support by the Austrian Science Fund (FWF, Project No. I 5111-N), the European Research Council (ERC Synergy Q-Xtreme), and by the European Union's Horizon 2020 research and innovation programme under Grant No. 863132 (iQLev).

[1] J. Millen, T. S. Monteiro, R. Pettit, and A. N. Vamivakas, Rep. Prog. Phys. **83**, 026401 (2020).
[2] C. Gonzalez-Ballestero, M. Aspelmeyer, L. Novotny, R. Quidant, and O. Romero-Isart, Science **374**, eabg3027 (2021).
[3] G. Ranjit, M. Cunningham, K. Casey, and A. A. Geraci, Phys. Rev. A **93**, 053801 (2016).
[4] D. Hempston, J. Vovrosh, M. Toroš, G. Winstone, M. Rashid, and H. Ulbricht, Appl. Phys. Lett. **111**, 133111 (2017).
[5] J. Ahn, Z. Xu, J. Bang, P. Ju, X. Gao, and T. Li, Nat. Nanotechnol. **15**, 89 (2020).
[6] M. Arndt and K. Hornberger, Nat. Phys. **10**, 271 (2014).
[7] J. Millen and B. A. Stickler, Contemp. Phys. **61**, 155 (2020).
[8] B. A. Stickler, K. Hornberger, and M. Kim, Nat. Rev. Phys. **3**, 589 (2021).
[9] H. Rudolph, K. Hornberger, and B. A. Stickler, Phys. Rev. A **101**, 011804(R) (2020).

[10] T. Krisnanda, G. Y. Tham, M. Paternostro, and T. Paterek, npj Quantum Inf. **6**, 12 (2020).
[11] S. Qvarfort, S. Bose, and A. Serafini, J. Phys. B **53**, 235501 (2020).
[12] A. A. Rakhubovsky, D. W. Moore, U. Delić, N. Kiesel, M. Aspelmeyer, and R. Filip, Phys. Rev. Appl. **14**, 054052 (2020).
[13] A. K. Chauhan, O. Černotík, and R. Filip, New J. Phys. **22**, 123021 (2020).
[14] F. Cosco, J. S. Pedernales, and M. B. Plenio, Phys. Rev. A **103**, L061501 (2021).
[15] T. Weiss, M. Roda-Llordes, E. Torrontegui, M. Aspelmeyer, and O. Romero-Isart, Phys. Rev. Lett. **127**, 023601 (2021).
[16] I. Brandão, D. Tandeitnik, and T. Guerreiro, Quantum Sci. Technol. **6**, 045013 (2021).
[17] D. C. Moore and A. A. Geraci, Quantum Sci. Technol. **6**, 014008 (2021).
[18] D. Carney, G. Krnjaic, D. C. Moore, C. A. Regal, G. Afek, S. Bhave, B. Brubaker, T. Corbitt, J. Cripe, N. Crisosto *et al.*, Quantum Sci. Technol. **6**, 024002 (2021).
[19] G. Afek, D. Carney, and D. C. Moore, Phys. Rev. Lett. **128**, 101301 (2022).
[20] S. Bose, A. Mazumdar, G. W. Morley, H. Ulbricht, M. Toroš, M. Paternostro, A. A. Geraci, P. F. Barker, M. S. Kim, and G. Milburn, Phys. Rev. Lett. **119**, 240401 (2017).
[21] C. Marletto and V. Vedral, Phys. Rev. Lett. **119**, 240402 (2017).
[22] H. Chevalier, A. J. Paige, and M. S. Kim, Phys. Rev. A **102**, 022428 (2020).
[23] D. Carney, H. Müller, and J. M. Taylor, PRX Quantum **2**, 030330 (2021).
[24] J. S. Pedernales, K. Streltsov, and M. B. Plenio, Phys. Rev. Lett. **128**, 110401 (2022).
[25] K. Streltsov, J. S. Pedernales, and M. B. Plenio, Universe **8**, 58 (2022).
[26] U. Delić, M. Reisenbauer, K. Dare, D. Grass, V. Vuletić, N. Kiesel, and M. Aspelmeyer, Science **367**, 892 (2020).
[27] L. Magrini, P. Rosenzweig, C. Bach, A. Deutschmann-Olek, S. G. Hofer, S. Hong, N. Kiesel, A. Kugi, and M. Aspelmeyer, Nature (London) **595**, 373 (2021).
[28] F. Tebbenjohanns, M. L. Mattana, M. Rossi, M. Frimmer, and L. Novotny, Nature (London) **595**, 378 (2021).
[29] A. Ranfagni, K. Børkje, F. Marino, and F. Marin, Phys. Rev. Res. **4**, 033051 (2022).
[30] M. Kamba, R. Shimizu, and K. Aikawa, Opt. Express **30**, 26716 (2022).
[31] U. Delić, M. Reisenbauer, D. Grass, N. Kiesel, V. Vuletić, and M. Aspelmeyer, Phys. Rev. Lett. **122**, 123602 (2019).
[32] D. Windey, C. Gonzalez-Ballestero, P. Maurer, L. Novotny, O. Romero-Isart, and R. Reimann, Phys. Rev. Lett. **122**, 123601 (2019).
[33] C. Gonzalez-Ballestero, P. Maurer, D. Windey, L. Novotny, R. Reimann, and O. Romero-Isart, Phys. Rev. A **100**, 013805 (2019).
[34] H. Rudolph, J. Schäfer, B. A. Stickler, and K. Hornberger, Phys. Rev. A **103**, 043514 (2021).
[35] N. Meyer, A. de los Rios Sommer, P. Mestres, J. Gieseler, V. Jain, L. Novotny, and R. Quidant, Phys. Rev. Lett. **123**, 153601 (2019).
[36] J. Schäfer, H. Rudolph, K. Hornberger, and B. A. Stickler, Phys. Rev. Lett. **126**, 163603 (2021).
[37] J. Vovrosh, M. Rashid, D. Hempston, J. Bateman, M. Paternostro, and H. Ulbricht, J. Opt. Soc. Am. B **34**, 1421 (2017).
[38] T. Seberson and F. Robicheaux, Phys. Rev. A **99**, 013821 (2019).
[39] G. P. Conangla, F. Ricci, M. T. Cuairan, A. W. Schell, N. Meyer, and R. Quidant, Phys. Rev. Lett. **122**, 223602 (2019).
[40] F. Tebbenjohanns, M. Frimmer, V. Jain, D. Windey, and L. Novotny, Phys. Rev. Lett. **124**, 013603 (2020).
[41] L. Dania, D. S. Bykov, M. Knoll, P. Mestres, and T. E. Northup, Phys. Rev. Res. **3**, 013018 (2021).
[42] F. van der Laan, F. Tebbenjohanns, R. Reimann, J. Vijayan, L. Novotny, and M. Frimmer, Phys. Rev. Lett. **127**, 123605 (2021).
[43] A. Setter, M. Toroš, J. F. Ralph, and H. Ulbricht, Phys. Rev. A **97**, 033822 (2018).
[44] C. Ockeloen-Korppi, E. Damskägg, J.-M. Pirkkalainen, M. Asjad, A. Clerk, F. Massel, M. Woolley, and M. Sillanpää, Nature (London) **556**, 478 (2018).
[45] R. Riedinger, A. Wallucks, I. Marinković, C. Löschnauer, M. Aspelmeyer, S. Hong, and S. Gröblacher, Nature (London) **556**, 473 (2018).
[46] I. Marinković, A. Wallucks, R. Riedinger, S. Hong, M. Aspelmeyer, and S. Gröblacher, Phys. Rev. Lett. **121**, 220404 (2018).
[47] T. Penny, A. Pontin, and P. Barker, arXiv:2111.03123.
[48] J. Rieser, M. A. Ciampini, H. Rudolph, N. Kiesel, K. Hornberger, B. A. Stickler, M. Aspelmeyer, and U. Delić, Science **377**, 987 (2022).
[49] J. Vijayan, Z. Zhang, J. Piotrowski, D. Windey, F. van der Laan, M. Frimmer, and L. Novotny, arXiv:2205.04455.
[50] See Supplemental Material at http://link.aps.org/supplemental/10.1103/PhysRevLett.129.193602 for a derivation of the feedback master equation, the modification of the particle equilibrium positions due to Coulomb interaction, and the technical details of solving the feedback master equation, including Refs. [51–56].
[51] J. D. Jackson, *Classical Electrodynamics* (Wiley, New York, 1999).
[52] H. M. Wiseman and G. J. Milburn, *Quantum Measurement and Control* (Cambridge University Press, Cambridge, England, 2009).
[53] W. P. Bowen and G. J. Milburn, *Quantum Optomechanics* (CRC Press, Boca Raton, 2015).
[54] M. G. A. Paris, F. Illuminati, A. Serafini, and S. De Siena, Phys. Rev. A **68**, 012314 (2003).
[55] G. Vidal and R. F. Werner, Phys. Rev. A **65**, 032314 (2002).
[56] M. Ludwig, K. Hammerer, and F. Marquardt, Phys. Rev. A **82**, 012333 (2010).
[57] K. Jacobs, *Quantum Measurement Theory and Its Applications* (Cambridge University Press, Cambridge, England, 2014).
[58] T. Seberson and F. Robicheaux, Phys. Rev. A **102**, 033505 (2020).
[59] F. Tebbenjohanns, M. Frimmer, A. Militaru, V. Jain, and L. Novotny, Phys. Rev. Lett. **122**, 223601 (2019).

[60] D. J. Wilson, V. Sudhir, N. Piro, R. Schilling, A. Ghadimi, and T. J. Kippenberg, Nature (London) **524**, 325 (2015).
[61] C. Li, Y. Li, H. Hu, and Y. Dong, Sci. China Phys. Mech. **65**, 240311 (2022).
[62] J. Eisert and M. B. Plenio, J. Mod. Opt. **46**, 145 (1999).
[63] C. Sommer and C. Genes, Phys. Rev. Lett. **123**, 203605 (2019).
[64] L. Martinetz, K. Hornberger, and B. A. Stickler, Phys. Rev. E **97**, 052112 (2018).